Magnetocaloric effect and critical behavior in arylamine-based copper chloride layered organic-inorganic perovskite

Septiany, Liany; Blake, Graeme R.

Published in:
Journal of Magnetism and Magnetic Materials

DOI:
10.1016/j.jmmm.2021.168598

Publication date:
2022

Journal of Magnetism and Magnetic Materials 542 (2022) 168598

Contents lists available at ScienceDirect

Journal of Magnetism and Magnetic Materials

journal homepage: www.elsevier.com/locate/jmmm

Research articles

Magnetocaloric effect and critical behavior in arylamine-based copper chloride layered organic-inorganic perovskite

Liany Septiany, Graeme R. Blake *

Zernike Institute for Advanced Materials, University of Groningen, Nijenborgh 4, 9747AG Groningen, Netherlands

ARTICLE INFO

Keywords:
Magnetocaloric
Critical behavior
Layered perovskite
2D ferromagnetism

ABSTRACT

Layered organic-inorganic hybrid perovskites have been the focus of much research regarding their optoelectronic and multiferroic properties. Here, we demonstrate the presence of a large magnetocaloric effect in the ferromagnetic layered perovskite phenylmethylammonium copper chloride ($(PMA)_2CuCl_4$) below the Curie temperature of ~9.5 K. We measure a magnetic entropy change ranging from 0.88 J/kg.K to 2.98 J/kg.K in applied fields of 10 kOe and 70 kOe, respectively. We also study the nature of the magnetic phase transition using critical isotherm analysis. The critical exponents are consistent with the 2D-XY spin model.

1. Introduction

Layered organic-inorganic hybrid perovskites have gained much attention over the past decade due to their tunable multifunctional properties applied to areas of research such as optoelectronics, ferroelectricity, and two-dimensional (2D) (anti)ferromagnetism [1–7]. Compared to their 3D counterparts, 2D perovskites have more structural freedom regarding the organic component of the material. Whereas only a limited set of small organic cations can be incorporated in 3D hybrid perovskites, much longer cations can be used in 2D perovskites [8–15]. This leads to an advantage of 2D perovskites that they are more stable under standard environmental conditions, mainly due to the hydrophobicity of the larger organic cations [16].

Recently, a large magnetic entropy change was observed in the 2D perovskites $(MA)_2CuCl_4$ [17], $(C_{12}H_{25}NH_3)_2CuCl_4$ [18], and $(C_2H_5NH_3)_2CoCl_4$ [19], with a magnitude comparable to that in all-inorganic compounds. Large magnetic entropy changes are related to the magnetocaloric effect which is important in magnetic refrigeration applications. The magnetocaloric effect (MCE) refers to a thermodynamic phenomenon where applying an external magnetic field under adiabatic conditions results in a temperature change in a magnetic material [20–24]. The MCE is an intrinsic property of a material and the largest effect is usually found close to magnetic phase transitions, particularly when associated with strong spin-lattice coupling at a paramagnetic to ferromagnetic phase transition. The compounds referred to above contain organic cations with linear alkyl chains, but a large number of 2D perovskites containing arylamine-based cations are also known. Many of these adopt polar crystal structures, leading to ferroelectric [25] and multiferroic [26] properties as well as 2D magnetism [27,28]. Here we show that the arylamine-based perovskite $(C_6H_5CH_2NH_3)_2CuCl_4$, referred to hereafter as $(PMA)_2CuCl_4$, also exhibits a large magnetocaloric effect. The ferromagnetic properties of $CuCl_4$-based perovskites were first investigated in the 1970 s using magnetization, electron paramagnetic resonance (EPR), and nuclear magnetic resonance (NMR) measurements [28–31]. $(PMA)_2CuCl_4$ was identified as a quasi-2D XY ferromagnet with $T_c \sim 8$ K. The J'/J ratio was determined to be $\sim 10^{-5}$, where J is the exchange constant between neighboring Cu^{2+} cations within a magnetic layer, and J' is the exchange constant between Cu^{2+} cations in adjacent layers, separated by bilayers of PMA cations.

The in-plane ferromagnetic interactions in $(PMA)_2CuCl_4$ arise due to the Jahn-Teller-active nature of the Cu^{2+} cation (d^9) in octahedral coordination. The degeneracy of the $d_{x^2-y^2}$ and d_{z^2} orbitals is lifted by an axial elongation of the $CuCl_6$ octahedra in the plane of the inorganic layers, which lowers the energy of the d_{z^2} orbital. The elongated Cu-Cl bonds are arranged in an antiferrodistortive manner in adjacent octahedra. Neighboring half-filled (magnetic) $d_{x^2-y^2}$ orbitals are therefore nearly orthogonal to each other, a configuration that gives rise to in-plane ferromagnetic superexchange via the Cl p-orbitals according to the Goodenough-Kanamori rules [32,33].

Despite the fact that an ideal 2D Heisenberg or XY magnet should not exhibit long-range ordering at any finite temperature, long-range 3D order is observed to take place in 2D hybrid perovskites [31]. The mechanism that induces such ordering may involve Ising anisotropy or

* Corresponding author.
E-mail address: g.r.blake@rug.nl (G.R. Blake).

https://doi.org/10.1016/j.jmmm.2021.168598
Received 22 June 2021; Received in revised form 26 August 2021; Accepted 23 September 2021
Available online 27 September 2021

the Dzyaloshinsky-Moriya interaction, which are of similar magnitude [34]. The weak interactions between the inorganic layers in 2D hybrid perovskites are usually antiferromagnetic in nature [31], with the exception of $(CH_3NH_3)_2CuCl_4$ and some analogues containing arylammonium cations, including $(PMA)_2CuCl_4$ [30,35], which are ferromagnetic. A recent report proposed that the interlayer coupling in $(PMA)_2CuCl_4$ is antiferromagnetic in fields of less than 1000 Oe (the easy axis lies in the inorganic plane, thus an antiferromagnetic signal can be observed when the field is applied in the out-of-plane direction) and becomes ferromagnetic in higher fields [36]. We also note that it was already pointed out by de Jongh and Miedema in 1974 that competition between interlayer couplings of different sign cannot be ruled out in 2D copper chloride–based perovskites [31], an issue that is difficult to investigate experimentally and to the best of our knowledge remains unresolved.

Here we demonstrate that the T_C of $(PMA)_2CuCl_4$ changes significantly with external field strength. A large magnetic entropy change is observed from the field dependence of the magnetization, ranging from 0.88 J/kg.K to 2.98 J/kg.K in applied fields of 10 kOe and 70 kOe, respectively. Furthermore, we study the critical behavior of the compound near T_C, which confirms the validity of the 2D XY spin model proposed in previous studies [35,37].

2. Materials and methods

An antisolvent method was used to synthesize $(PMA)_2CuCl_4$ crystals. First, the precursor salt phenylmethylammonium chloride (PMACl) was prepared. A 1:1 M ratio of phenylmethylamine (Sigma Aldrich, for synthesis) and HCl was mixed in ethanol (1.25 M, Sigma Aldrich) as a solvent and left to dry at 60 °C on a hot plate. The white powder obtained was washed three times with diethyl ether (Macron Chemicals) and vacuum dried overnight. For the growth of $(PMA)_2CuCl_4$ crystals, a 1:2 M ratio of PMACl and anhydrous $CuCl_2$ (Alfa Aesar, 98%) was dissolved in a separate flask with methanol as the solvent. The two solutions were mixed and stirred for ~2 h. A two-layer solution was then prepared by slowly adding acetonitrile (Sigma Aldrich, anhydrous 99.8%) on top of the methanol solution and was placed in a 40 °C water bath. The solution was left to evaporate for 3–4 days. We obtained two different products from the synthesis: $(PMA)_2CuCl_4$ crystals in the form of brown platelets, and dark green needles that were identified by single-crystal X-ray diffraction as an oxido-copper cluster compound, a member of the family with general formula $Cu_4OX_6(L')_4$ (X = halide, L′ = ligand), in this case with X = Cl and L′ = PMA [38–40].

Single-crystal X-ray diffraction (XRD) measurements were carried out using a Bruker D8 Venture diffractometer with Mo-Kα radiation. The crystal was mounted in a fiber loop using cryo-oil. The measurement temperature was controlled by a nitrogen flow using an Oxford Cryostream Plus. Data were processed using the Bruker APEX III software. Structure solution was carried out using direct methods and refinement was performed using the SHELXTL software. In addition, powder XRD measurement was carried out on hand-ground $(PMA)_2CuCl_4$ crystals using a Bruker D8 Advance diffractometer equipped with a Cu Kα-source.

A Quantum Design MPMS SQUID magnetometer was used to carry out the magnetic measurements. Several single crystals were stacked together such that measurements were performed with the magnetic field applied in-plane. The temperature dependence of the DC magnetization was measured from 5 to 300 K in various fields ranging from 5 Oe to 1 kOe. AC magnetization measurements were carried out from 2 to 25 K using an AC field of 3.8 Oe superimposed on a DC field of 200 Oe. Isothermal magnetization versus field measurements were performed from +70 kOe to −70 kOe at 1 K intervals between 5 and 30 K.

3. Results and discussion

3.1. Crystal structure

Previous studies of $(PMA)_2CuCl_4$ based on powder XRD data reported that the crystal structure is orthorhombic at room temperature, with space group *Pbca* [28,36]. Here, our single-crystal XRD data indicate that the symmetry is monoclinic with space group *Cc* between 100 K and room temperature (Fig. 1). The associated structural parameters at 100 and 300 K are presented in Table 1.

Reciprocal lattice images reconstructed from raw data are given in Fig. S1. The reflection condition for a C-centered lattice is observed: *hkl*, $h + k = 2n$. The condition *h*0*l*, $l = 2n$ is also observed and corresponds to a *c*-glide plane perpendicular to the *b*-axis. This implies the space groups *C*2/*c* or *Cc*, and the structure could only be solved in the latter space group. In the 0*kl* plane (Fig. S1(a)) many extra spots with half-integer values of *k* are observed, which suggests that the *b*-axis is doubled. However, these spots are projections of the rather diffuse, streaky rows of spots with half-integer *k* apparent in the *hk*0 projection (Fig. S1(c)). Therefore, the doubled *b*-axis probably corresponds to order that is rather short-range in nature. Attempts to solve the structure in an $a \times 2b \times c$ unit cell were unsuccessful. The presence of this supercell implies that our solved structure should be considered an average structure only, and the rather high fit factors R1 and wR2 also suggest that the detailed structure is more complex.

We also carried out powder XRD on a sample comprised of crushed crystals, as shown in Fig. S2. The allowed peak positions associated with the single-crystal XRD structure are indicated and match well with the measured peaks. The pattern shows a strong preferred orientation along the layer stacking direction [*h* 0 0] due to the plate-like morphology of the crystals, manifested by a high intensity on the corresponding peaks. Impurity peaks are observed, especially below $2\theta = 15°$, and correspond to the oxido-copper cluster compound mentioned above.

3.2. Magnetic measurements

The temperature dependent DC magnetization of $(PMA)_2CuCl_4$ was measured in field-cooled mode from 5 to 300 K with various in-plane applied magnetic fields (Fig. 2(a)). The significant increase in magnetization below ~10 K suggests the onset of ferromagnetic ordering. This is supported by the S-shaped magnetization versus applied field curve measured at 10 K (Fig. 2(b)). No hysteresis is observed. The transition temperature, T_C, is in the range 8–10 K depending on the magnitude of the external magnetic field applied up to 200 Oe, as determined from the sharp peak in the differential magnetization curve in the inset of Fig. 2 (a). Fig. S4 shows the AC magnetization as a function of temperature, where a frequency-independent peak at 9.5 K is observed in the real component χ' when measured in an underlying DC field of 200 Oe, which agrees with the DC magnetization in Fig. 2(a). A corresponding

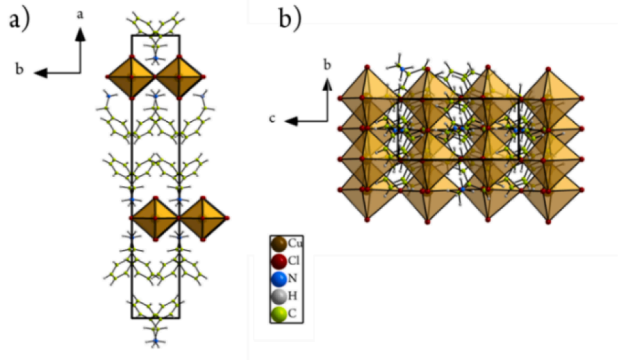

Fig. 1. Structure of $(PMA)_2CuCl_4$ viewed along a) *c*-axis and b) *a*-axis.

Table 1
Structural parameters of $(PMA)_2CuCl_4$ measured at 100 K and 300 K.

	100 K	300 K
Crystal system	Monoclinic	
Space group	*Cc*	
a (Å)	31.436(3)	31.846(7)
b (Å)	5.2247(5)	5.2624(11)
c (Å)	10.4816(12)	10.588(2)
β (°)	99. 379(7)	98.553(9)
V (Å^3)	1698.5	1754.72
ρ(g/cm^3)	1.649	1.596
Absorption coeff. (mm^{-1})	1.91	1.85
f (000)	860	860
Index ranges	$-38\leq h\leq 38$,	$-34\leq h\leq 34$,
	$-6\leq k\leq 6$,	$-13\leq l\leq 13$
	$-5\leq k\leq 5$,	$-11\leq l\leq 11$
Goodness of fit	1.083	1.0692
R indices	wR2 = 0.2898	wR2 = 0.1887
	R1 = 0.1024	R1 = 0.0586
Largest diff. peak/hole (e/Å^3)	2.63/−2.18	1.15/−1.59

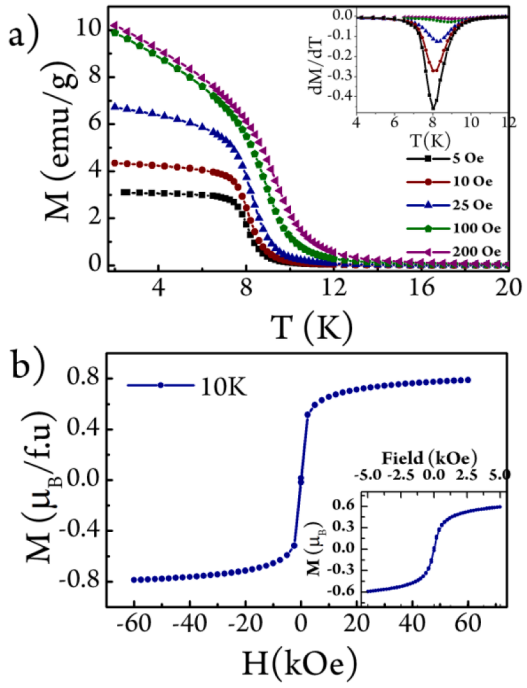

Fig. 2. a) Temperature dependence of field-cooled in-plane magnetization of $(PMA)_2CuCl_4$ measured in low applied fields; the inset shows the derivative dM/dT versus temperature. b) Field dependent magnetization at 10 K; the inset shows the low-field region.

peak is also present in the imaginary part χ" of the AC magnetization; such a peak is related to irreversible magnetization processes and is consistent with ferromagnetic ordering involving the rearrangement of domain walls.

Curie-Weiss fitting to the inverse DC susceptibility data in the temperature range above 150 K (Fig. S3) yields a positive Curie-Weiss temperature (θ_{CW}) of 71.7 K. This large, positive value of θ_{CW} compared to the 3D ordering temperature T_C shows that in-plane 2D ferromagnetic interactions are strong. The effective magnetic moment is determined as $\mu_{eff} = 1.44\ \mu_B$, which is slightly smaller than the theoretical spin-only value for Cu^{2+} of 1.73 μ_B. We note that the curve is not perfectly linear over the temperature range measured.

3.3. Magnetocaloric effect

The field-dependence of T_C that is apparent in Fig. 2(a) suggests the presence of a significant magnetic entropy change at the onset of ferromagnetic ordering, which is a desirable characteristic of magnetocaloric materials. In addition to a large magnetic entropy change, good magnetocaloric materials exhibit minimal losses on cycling the temperature or magnetic field, thus a second-order magnetic phase transition is desirable. As shown by the field-dependent magnetization in Fig. 2(b), we do not observe any hysteresis, which suggests a second-order nature. The order of the magnetic phase transition can be probed using an Arrot plot, which shows the relation between the square of the magnetization (M^2) and H/M obtained from a series of isothermal magnetization versus field measurements, as shown in Fig. 3(b) [41]. According to the Banerjee criterion, a positive slope is obtained for materials that exhibit a second-order phase transition, while a negative slope corresponds to a first-order transition [42]. Our plots exhibit positive slopes for the temperature range from 5 to 30 K, which suggests a second-order phase transition.

Isothermal magnetization versus applied field data also allow us to calculate the magnetic entropy changes that arise due to the applied field. Field-dependent magnetization measurements were carried out in the range 0–70 kOe at constant temperatures from 5 to 30 K (shown in Fig. 3(a)). By using Maxwell's equation, the entropy change ΔS can be calculated as [20]:

$$\left(\frac{\partial S}{\partial T}\right)_T = \left(\frac{\partial M}{\partial T}\right)_H \quad (1)$$

$$\Delta S(T,H) = \int_0^H \left(\frac{\partial M}{\partial T}\right)_H dH \quad (2)$$

The magnetic entropy change plot in Fig. 4(a) exhibits a series of maxima that shift to higher temperatures as the magnetic field is increased, due to enhancement of the ferromagnetic interactions. The maximum entropy change, ΔS_M, ranges from 0.88 J/kg.K to 2.98 J/kg.K for applied fields increasing from 10 kOe to 70 kOe, respectively.

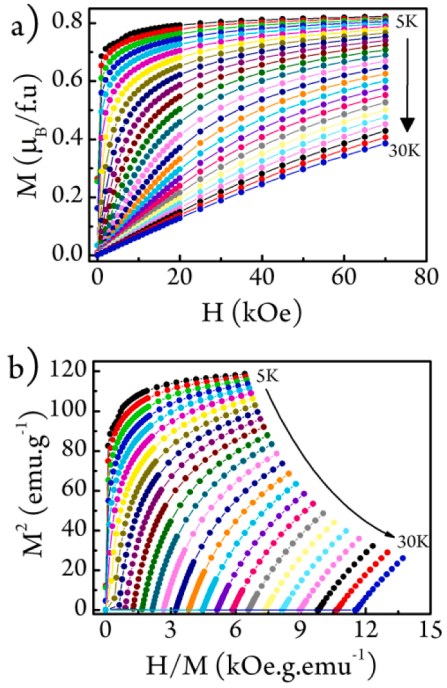

Fig. 3. a) Isothermal magnetization versus applied field curves measured at temperatures from 5 to 30 K. b) Corresponding Arrot plot, suggesting a second-order magnetic phase transition.

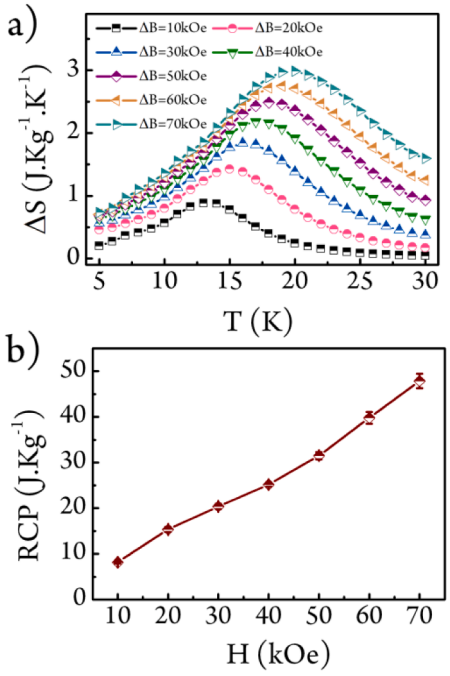

Fig. 4. a) Magnetic entropy change as a function of temperature at different applied fields. b) Relative cooling power (RCP) as a function of applied magnetic field.

The performance of a magnetocaloric material as a coolant is often quantified by the relative cooling power (RCP), which is the ability to interchange heat between a cold and hot region in one ideal refrigeration cycle and is given by [20],

$$RCP = \left|\Delta S_M^{Max}\right| \times \delta T_{FWHM} \tag{3}$$

Here δT_{FWHM} is the full-width at half maximum of the magnetic entropy change curve, which was determined from Gaussian fits to the curves in Fig. 4(a). As shown in Fig. 4(b), we obtained RCP values of up to 47.8 J/kg at 70 kOe, the highest magnetic field applied.

In Table 2 we compare the ΔS_M value of our compound at 70 kOe to other 2D perovskites in which the magnetocaloric properties have been investigated. Based on the limited evidence of only three other reports [17–19], it is possible that the value of ΔS_M increases for smaller interlayer spacing (using shorter organic cations such as CH_3NH_3 or $C_2H_5NH_3$), but further investigations are necessary to confirm this trend. The significantly larger ΔS_M reported for $(C_2H_5NH_3)_2CoCl_4$ is likely due to the larger spin of Co^{2+} (S = 3/2) compared to Cu^{2+} (S = 1/2).

Although the magnetocaloric properties of $(PMA)_2CuCl_4$ have not previously been studied, a recent report focused on magnetodielectric (MD) coupling in the same compound [36]. It was proposed that the MD coupling is associated with a change from antiferromagnetic to ferromagnetic interlayer coupling as the magnitude of the external field is increased above ~1 kOe. Similar to our current study, a magnetic moment of ~0.5 μ_B/f.u. was measured in an applied field of 3 kOe at 12 K, implying a considerable shift in T_C with field. Other Cu- and Mn-based 2D hybrid perovskites containing arylamine-based organic cations are also known to show magnetic field-induced spin reorientations [8,11] below T_C or T_N. The weak interlayer coupling and soft ferromagnetism in the case of Cu-based 2D perovskites allow the reorientation of spins by relatively low fields, thus resulting in large magnetic entropy changes.

Table 2
Magnetic entropy change (ΔS_M) of $(PMA)_2CuCl_4$ in 70 kOe applied field compared to other compounds with similar T_C.

Compound	Tc (K)	ΔS_M (J/kg.K)
$(C_6H_5CH_2NH_3)_2CuCl_4$ (our work)	9.5	2.98 (7 T)
$(CH_3NH_3)_2CuCl_4$ [17]	8.9	4.98 (5 T)
$(C_{12}H_{25}NH_3)_2CuCl_4$ [18]	13	1.90 (5 T)
$(C_2H_5NH_3)_2CoCl_4$ [19]	2	14.5 (7 T)

3.4. Critical behavior

The critical behavior of a magnetic material near the Curie temperature associated with a second-order transition can be characterized by a series of critical exponents according to the universal scaling hypothesis. These critical exponents β, γ, and δ can be determined from the spontaneous magnetization $M_S(T)$, initial susceptibility $\chi_0(T)$, and magnetization $M(H)$. The definitions of these exponents are as follows [43,44]:

$$M_s(T) = M_0(-\varepsilon)^{\beta}, \quad \varepsilon < 0, \quad T < T_c \tag{4}$$

$$\chi_0{}^{-1} = \frac{h_0}{m_0}\varepsilon^{\gamma}, \quad \varepsilon > 0, \quad T > T_c \tag{5}$$

$$M = DH^{1/\delta}, \quad \varepsilon = 0, \quad T = T_c \tag{6}$$

Here $\varepsilon = ((T - T_C)/T_C)$ is the reduced temperature, while M_0, h_0/m_0, and D are the critical amplitudes. Furthermore, using the scaling hypothesis, the relationship between the variables can be expressed as

$$M(H, \varepsilon) = \varepsilon_f^{\beta} \pm (H/\varepsilon^{\beta+\gamma}) \tag{7}$$

where the two terms are added for $T > T_C$ and subtracted for $T < T_C$. The renormalized magnetization $m \equiv \varepsilon^{-\beta}M(H, \varepsilon)$ and the renormalized field $h \equiv \varepsilon^{-(\beta+\gamma)}H$ should follow two universal rules that differentiate the behavior where $T < T_C$ and $T > T_C$.

Generally, Arrot plot analysis can be used to obtain the critical exponents and critical temperature. The Arrot plot presumes that the critical exponents follow mean-field theory where $\beta = 0.5$ and $\gamma = 1.0$, such that the M^2 vs H/M plots should consist of a set of a parallel straight lines. The plot corresponding to the critical temperature T_C should then pass through the origin. The intercepts with the M^2 axis and the H/M axis at any particular temperature should give the spontaneous magnetization $M_s(T)$ and initial susceptibility $\chi_o(T)$, respectively. As shown in Fig. 3(b), the Arrot plot does not consist of straight lines, which indicates that mean-field theory is not valid for our system.

A modified Arrot plot was then used to estimate the critical exponents of $(PMA)_2CuCl_4$. A set of known critical exponents from different models were used. The modified Arrot plot was constructed using the Arrot-Noakes equation of state [45]:

$$(H/M)^{1/\gamma} = a\left(\frac{T - T_c}{T_c}\right) + bM^{1/\beta} \tag{8}$$

Here the parameters a and b are considered constant. The plot of $(H/M)^{1/\gamma}$ vs $M^{1/\beta}$ should consist of a set of parallel straight lines if the correct set of critical exponents are chosen. Fig. S4 presents modified Arrot plots for several 3D models: the 3D Heisenberg, 3D XY, 3D Ising, and tricritical mean-field model [46,47]. None of the plots consist of parallel straight lines, which implies that the 3D models are invalid. This observation is not unexpected, as it is known that $(PMA)_2CuCl_4$ possesses 2D characteristics. Therefore, we next used critical exponents that were previously determined for the 2D Ising model [48]; the corresponding plot is shown in Fig. 5(a). In contrast to the 3D models, the 2D Ising model yields a set of curves that are almost linear, consistent with 2D characteristics.

To estimate the critical exponents of our system, we first used the critical isotherm approximation as stated in Eq. (6) to obtain δ. We plotted ln(M) vs ln(H); the slope of this graph gives us $1/\delta$. To obtain the β exponent the field dependence of the magnetic entropy change can be used, as stated in the equation below [44,49,50]:

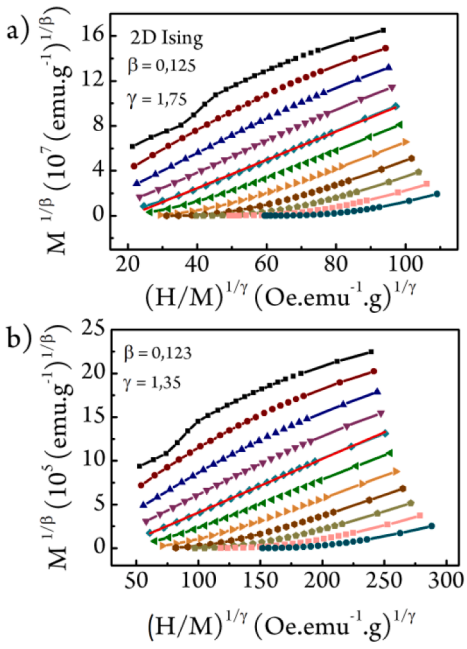

Fig. 5. Modified Arrot-Noakes plots for a) 2D Ising model and b) with γ and β values obtained from the critical isotherm approximation presented in Eqs. (6) and (9).

$$\Delta S_{m|_{T=T_c}} \propto H^n; \quad n = 1 + \frac{1}{\delta}\left(1 - \frac{1}{\beta}\right) \tag{9}$$

A plot of ΔS_m versus H on a log-log scale should be linear, where the slope gives the value of n. The two plots are presented in Fig. 6(a) and (b), respectively. Since δ is obtained from Fig. 6(a), the value of β can be extracted from Fig. 6(b). The γ exponent can then be calculated by Widom scaling where $\delta = 1 + \gamma/\beta$ [51].

Finally, we constructed a modified Arrot-Noakes plot using the extracted critical exponents, shown in Fig. 5(b). The curves are close to linear at temperatures around T_C, and the plot corresponding to T_C intercepts the origin. The values of exponents $\beta = 0.123$ and $\gamma = 1.35$ are close to those for the known 2D Ising model ($\beta = 0.125$ and $\gamma = 1.75$) [48]. Previously, Kosterlitz found that the critical exponents for the 2D XY and 2D Ising models are similar [52]. Since $(PMA)_2CuCl_4$ has previously been described as a 2D XY magnet, our results are consistent with these previous findings.

The reliability of the critical exponents can be tested using Eq. (4), such that the renormalized magnetization vs renormalized field graph should show different behavior below and above T_C. This is indeed the case as shown in Fig. 7 where a splitting of the curves is observed in the low field region. The inset of Fig. 7 shows the same plot on a log-log scale, where the splitting is more pronounced

4. Conclusions

We have restudied the crystal structure of $(PMA)_2CuCl_4$ and find that it crystallizes in the monoclinic, non-centrosymmetric space group *Cc* instead of the previously reported orthorhombic *Pbca* structure. Magnetization measurements show ferromagnetic ordering below $T_C = 9.5$ K, in agreement with previous reports. We demonstrate a large magnetocaloric effect by determining a magnetic entropy change, ΔS_M, that ranges from 0.88 J/kg.K to 2.98 J/kg.K for fields of 10 kOe to 70 kOe, respectively. The corresponding relative cooling power reaches a maximum of 47.8 J/kg in a field of 70 kOe. The large magnetic entropy change in $(PMA)_2CuCl_4$ indicates the potential of layered organic-inorganic perovskites for use in solid-state cooling devices. We have also investigated the behavior of $(PMA)_2CuCl_4$ in the vicinity of T_C by

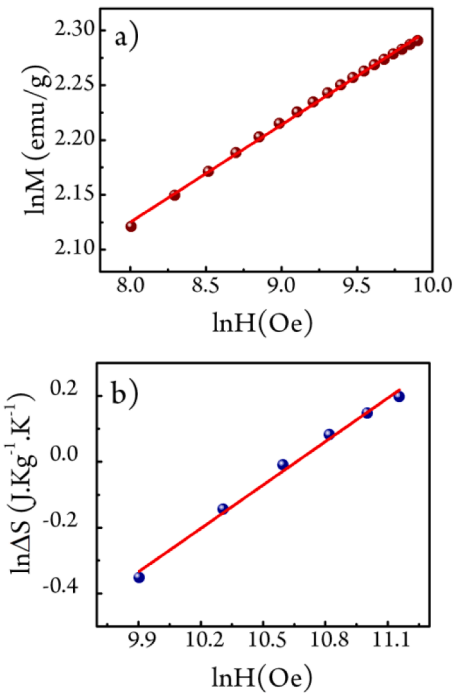

Fig. 6. a) Magnetization vs applied field on a log-log scale measured at T_C; the solid line is a linear fit to Eq. (6). b) Field dependence of magnetic entropy change at T_C on a log-log scale; the solid line represents a linear fit to Eq. (8).

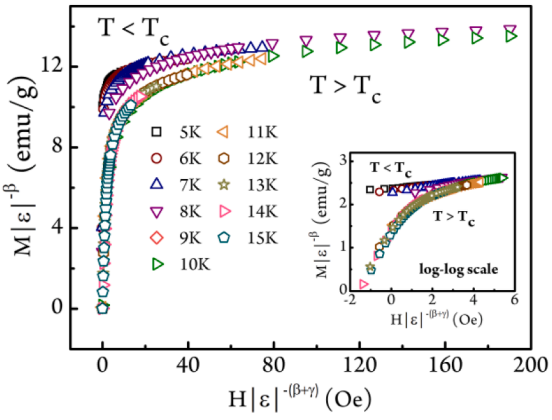

Fig. 7. Logarithmic scaling plot used to check the reliability of the critical exponents obtained, showing two different trends for $T < T_C$ and $T > T_C$.

determining the critical exponents using the critical isotherm approximation. Values of $\gamma = 1.45$, $\beta = 0.123$, and $\delta = 12.76$ are obtained, which are consistent with critical exponents expected for the 2D XY model.

CRediT authorship contribution statement

Liany Septiany: Conceptualization, Methodology, Validation, Formal analysis, Investigation, Data curation, Writing - original draft, Visualization, Project administration. **Graeme R. Blake:** Conceptualization, Validation, Resources, Data curation, Writing - review & editing, Supervision, Project administration.

Declaration of Competing Interest

The authors declare that they have no known competing financial interests or personal relationships that could have appeared to influence the work reported in this paper.

Acknowledgments

L. Septiany thanks the Indonesian Endowment Fund for Education (LPDP) for supporting her PhD study. We would like to thank Joshua Levinsky for valuable help in data analysis and Ing. Jacob Baas for technical support.

Appendix A. Supplementary data

Supplementary data to this article can be found online at https://doi.org/10.1016/j.jmmm.2021.168598.

References

[1] L. Pedesseau, D. Sapori, B. Traore, R. Robles, H.-H. Fang, M.A. Loi, H. Tsai, W. Nie, J.-C. Blancon, A. Neukirch, S. Tretiak, A.D. Mohite, C. Katan, J. Even, M. Kepenekian, Advances and promises of layered halide hybrid perovskite semiconductors, ACS Nano 10 (11) (2016) 9776–9786, https://doi.org/10.1021/acsnano.6b05944.

[2] M.D. Smith, B.A. Connor, H.I. Karunadasa, Tuning the luminescence of layered halide perovskites, Chem. Rev. 119 (5) (2019) 3104–3139, https://doi.org/10.1021/acs.chemrev.8b00477.

[3] T.D. Huan, V.N. Tuoc, N.V. Minh, Layered structures of organic/inorganic hybrid halide perovskites, Phys. Rev. B 93 (2016), 094105, https://doi.org/10.1103/PhysRevB.93.094105.

[4] M.D. Smith, E.J. Crace, A. Jaffe, H.I. Karunadasa, The diversity of layered halide perovskites, Annu. Rev. Mater. Res. 48 (1) (2018) 111–136, https://doi.org/10.1146/annurev-matsci-070317-124406.

[5] Z. Cheng, J. Lin, Layered organic-inorganic hybrid perovskites: Structure, optical properties, film preparation, patterning and templating engineering, CrystEngComm 12 (2010) 2646–2662, https://doi.org/10.1039/c001929a.

[6] N.A. Benedek, J.M. Rondinelli, H. Djani, P. Ghosez, P. Lightfoot, Understanding ferroelectricity in layered perovskites: new ideas and insights from theory and experiments, Dalton Trans. 44 (2015) 10543–10558, https://doi.org/10.1039/c5dt00010f.

[7] L. Mao, C.C. Stoumpos, M.G. Kanatzidis, Two-Dimensional Hybrid halide perovskites: principles and promises, J. Am. Chem. Soc. 141 (3) (2019) 1171–1190, https://doi.org/10.1021/jacs.8b10851.

[8] S.-H. Park, I.-H. Oh, S. Park, Y. Park, J.H. Kim, Y.-D. Huh, Canted antiferromagnetism and spin reorientation transition in layered inorganic–organic perovskite $(C_6H_5CH_2CH_2NH_3)_2MnCl_4$, Dalton Trans. 41 (4) (2012) 1237–1242, https://doi.org/10.1039/C1DT11544H.

[9] G. Park, I.H. Oh, J.M.S. Park, J. Jung, C.Y. You, J.S. Kim, Y. Kim, J.H. Jung, N. Hur, Y. Kim, J.Y. Kim, C.S. Hong, K.Y. Kim, Solvent-dependent self-assembly of two dimensional layered perovskite $(C_6H_5CH_2CH_2NH_3)_2MCl_4$ (M = Cu, Mn) thin films in ambient humidity, Sci. Rep. 8 (2018) 466, https://doi.org/10.1038/s41598-018-23012-2.

[10] S.Y. Kim, J.M. Yang, E.S. Choi, N.G. Park, Layered $(C_6H_5CH_2NH_3)_2CuBr$ 4 perovskite for multilevel storage resistive switching memory, Adv. Funct. Mater. 30 (2020) 2002653, https://doi.org/10.1002/adfm.202002653.

[11] B.o. Huang, J.-Y. Zhang, R.-K. Huang, M.-K. Chen, W. Xue, W.-X. Zhang, M.-H. Zeng, X.-M. Chen, Spin-reorientation-induced magnetodielectric coupling effects in two layered perovskite magnets, Chem. Sci. 9 (37) (2018) 7413–7418, https://doi.org/10.1039/C8SC02917B.

[12] A.A. Nugroho, Z. Hu, C.Y. Kuo, M.W. Haverkort, T.W. Pi, D. Onggo, M. Valldor, L. H. Tjeng, Cross-type orbital ordering in the layered hybrid organic-inorganic compound $(C_6H_5CH_2CH_2NH_3)_2CuCl_4$, Phys. Rev. B 94 (2016), 184404, https://doi.org/10.1103/PhysRevB.94.184404.

[13] M.E. Kamminga, R. Hidayat, J. Baas, G.R. Blake, T.T.M. Palstra, Out-of-plane polarization in a layered manganese chloride hybrid, APL Mater. 6 (2018), 066106, https://doi.org/10.1063/1.5024857.

[14] L. Zou, H.X. Liu, L.L. Guo, G.T. Xu, G.F. Xue, Preparation and characterization of organic-inorganic hybrid perovskite $(C_6H_5CH_2NH_3)_2CuCl_4$, Adv. Mater. Res. 311–313 (2011) 2146–2150, https://doi.org/10.4028/www.scientific.net/AMR.311-313.2146.

[15] P. Zhou, J.E. Drumheller, B. Patyal, R.D. Willett, Magnetic properties and critical behavior of quasi-two-dimensional systems $[C_6H_5(CH_2)_nNH_3]_2CuBr$ 4 with n = 1, 2, and 3, Phys. Rev. B. 45 (1992) 12365–12376, https://doi.org/10.1103/PhysRevB.45.12365.

[16] M.I. Asghar, J. Zhang, H. Wang, P.D. Lund, Device stability of perovskite solar cells – a review, Renew. Sustain. Energy Rev. 77 (2017) 131–146, https://doi.org/10.1016/j.rser.2017.04.003.

[17] Y. Ma, K. Zhai, L. Yan, Y. Chai, D. Shang, Y. Sun, Magnetocaloric effect in the layered organic-inorganic hybrid $(CH_3NH_3)_2CuCl_4$, Chin. Phys. B 27 (2018), 027501, https://doi.org/10.1088/1674-1056/27/2/027501.

[18] M. Bochalya, S. Kumar, Magnetocaloric effect in 2D-alkylammonium copper halides layered inorganic-organic systems, J. Appl. Phys. 127 (2020), 055501, https://doi.org/10.1063/1.5134102.

[19] A. Sen, S. Roy, S.C. Peter, A. Paul, U.V. Waghmare, A. Sundaresan, Order-disorder structural phase transition and magnetocaloric effect in organic-inorganic halide hybrid $(C_2H_5NH_3)_2CoCl_4$, J. Solid State Chem. 258 (2018) 431–440, https://doi.org/10.1016/j.jssc.2017.10.036.

[20] K.A. GschneidnerJr, V.K. Pecharsky, A.O. Tsokol, Recent developments in magnetocaloric materials, Rep. Prog. Phys. 68 (6) (2005) 1479–1539, https://doi.org/10.1088/0034-4885/68/6/R04.

[21] V.K. Pecharsky, K.A. Gschneidner, Magnetocaloric effect and magnetic refrigeration, J. Magn. Magn. Mater. 200 (1-3) (1999) 44–56, https://doi.org/10.1016/S0304-8853(99)00397-2.

[22] V. Zverev, A.M. Tishin, Magnetocaloric Effect: From Theory to Practice, Elsevier Ltd. (2016), https://doi.org/10.1016/b978-0-12-803581-8.02813-7.

[23] K.A. Gschneidner, V.K. Pecharsky, Thirty years of near room temperature magnetic cooling: Where we are today and future prospects, Int. J. Refrig. 31 (2008) 945–961, https://doi.org/10.1016/j.ijrefrig.2008.01.004.

[24] K.G. Sandeman, Magnetocaloric materials: the search for new systems, Scr. Mater. 67 (6) (2012) 566–571, https://doi.org/10.1016/j.scriptamat.2012.02.045.

[25] S. Shahrokhi, W. Gao, Y. Wang, P.R. Anandan, M.Z. Rahaman, S. Singh, D. Wang, C. Cazorla, G. Yuan, J.M. Liu, T. Wu, Emergence of ferroelectricity in halide perovskites, Small Methods 4 (2020) 2000149, https://doi.org/10.1002/smtd.202000149.

[26] A.O. Polyakov, A.H. Arkenbout, J. Baas, G.R. Blake, A. Meetsma, A. Caretta, P.H. M. van Loosdrecht, T.T.M. Palstra, Coexisting ferromagnetic and ferroelectric order in a $CuCl_4$-based organic-inorganic hybrid, Chem. Mater. 24 (1) (2012) 133–139, https://doi.org/10.1021/cm2023696.

[27] G. Park, I.H. Oh, J.M.S. Park, S.H. Park, C.S. Hong, K.S. Lee, Investigation of magnetic phase transition on the layered inorganic-organic hybrid perovskites by single-crystal neutron diffraction, Physica B 551 (2018) 89–93, https://doi.org/10.1016/j.physb.2017.11.004.

[28] A. Dupas, K. Le Dang, J.-P. Renard, P. Veillet, A. Daoud, R. Perret, Magnetic properties of the nearly two-dimensional ferromagnets $[C_6H_5(CH_2)_nNH_3]_2CuCl_4$ with n=1,2,3, J. Chem. Phys. 65 (10) (1976) 4099–4102, https://doi.org/10.1063/1.432864.

[29] Y. Kimishima, Magnetic phase transitions in $(C_6H_5CH_2NH_3)_2CuCl_4$, J. Magn. Magn. Mater. 90–91 (1990) 301–302, https://doi.org/10.1016/S0304-8853(10)80108-8.

[30] W.E. Estes, D.B. Losee, W.E. Hatfield, The magnetic properties of several quasi two-dimensional Heisenberg layer compounds: a new class of ferromagnetic insulators involving halocuprates, J. Chem. Phys. 72 (1980) 630–638, https://doi.org/10.1063/1.438953.

[31] L.J. de Jongh, A.R. Miedema, Experiments on simple magnetic model systems, Adv. Phys. 23 (1) (1974) 1–260, https://doi.org/10.1080/00018739700101558.

[32] J.B. Goodenough, Theory of the role of covalence in the perovskite-type manganites [La, M(II)]MnO_3, Phys. Rev. 100 (1955) 564–573, https://doi.org/10.1103/PhysRev.100.564.

[33] J. Kanamori, Superexchange interaction and symmetry properties of electron orbitals, J. Phys. Chem. Solids 10 (2-3) (1959) 87–98, https://doi.org/10.1016/0022-3697(59)90061-7.

[34] K.W. Lee, C.H. Lee, C.E. Lee, J.K. Kang, Magnetic ordering in two-dimensional Heisenberg antiferromagnets with variable interlayer distances, Phys. Rev. B 62 (1) (2000) 95–98, https://doi.org/10.1103/PhysRevB.62.95.

[35] Y. Kimishima, Successive phase transitions in 2D-XY ferromagnet $(C_6H_5CH_2NH_3)_2CuCl_4$, Jpn. J. Appl. Phys. 26 (1987) 867–868, https://doi.org/10.7567/JJAPS.26S3.867.

[36] Y.H. Kim, N. Hur, Magnetic properties and magnetodielectric effect in $(C_6H_5CH_2NH_3)_2[CuCl_4]$ with organic-inorganic hybrid layered structure, J. Korean Phys. Soc. 77 (11) (2020) 1026–1030, https://doi.org/10.3938/jkps.77.1026.

[37] H. Han, L. Zhang, X. Zhu, H. Du, M. Ge, L. Ling, L. Pi, C. Zhang, Y. Zhang, Anisotropic magnetic coupling with a two-dimensional characteristic in noncentrosymmetric $Cr_{11}Ge_{19}$, Sci. Rep. 6 (2016) 39338, https://doi.org/10.1038/srep39338.

[38] S. Becker, M. Dürr, A. Miska, J. Becker, C. Gawlig, U. Behrens, I. Ivanović-Burmazović, S. Schindler, Copper chloride catalysis: do μ_4-oxido copper clusters play a significant role? Inorg. Chem. 55 (2016) 3759–3766, https://doi.org/10.1021/acs.inorgchem.5b02576.

[39] S. Becker, U. Behrens, S. Schindler, Investigations concerning $[Cu_4OX_6L_4]$ cluster formation of copper(II) chloride with amine ligands related to benzylamine, Eur. J. Inorg. Chem. 2015 (14) (2015) 2437–2447, https://doi.org/10.1002/ejic.201500115.

[40] S. Löw, J. Becker, C. Würtele, A. Miska, C. Kleeberg, U. Behrens, O. Walter, S. Schindler, Reactions of copper(II) chloride in solution: facile formation of tetranuclear copper clusters and other complexes that are relevant in catalytic redox processes, Chem. Eur. J. 19 (2013) 5342–5351, https://doi.org/10.1002/chem.201203848.

[41] A. Arrott, Criterion for ferromagnetism from observations of magnetic isotherms, Phys. Rev. 108 (6) (1957) 1394–1396, https://doi.org/10.1103/PhysRev.108.1394.

[42] B.K. Banerjee, On a generalised approach to first and second order magnetic transitions, Phys. Lett. 12 (1) (1964) 16–17, https://doi.org/10.1016/0031-9163(64)91158-8.

[43] H.E. Stanley, Scaling, universality, and renormalization: three pillars of modern critical phenomena, Rev. Mod. Phys. 71 (1999) 358–366, https://doi.org/10.1103/revmodphys.71.s358.

[44] R. Pełka, P. Konieczny, M. Fitta, M. Czapla, P.M. Zieliński, M. Bałanda, T. Wasiutyński, Y. Miyazaki, A. Inaba, D. Pinkowicz, B. Sieklucka, Magnetic systems at criticality: different signatures of scaling, Acta Phys. Pol. A 124 (6) (2013) 977–989.

[45] A. Arrott, J.E. Noakes, Approximate equation of state for nickel near its critical temperature, Phys. Rev. Lett. 19 (14) (1967) 786–789, https://doi.org/10.1103/PhysRevLett.19.786.

[46] S.N. Kaul, Static critical phenomena in ferromagnets with quenched disorder, J. Magn. Magn. Mater. 53 (1-2) (1985) 5–53, https://doi.org/10.1016/0304-8853(85)90128-3.
[47] K. Huang, Statistical Mechanics, second Ed., Wiley, New York, 1991.
[48] J.C. Le Guillou, J. Zinn-Justin, Critical exponents from field theory, Phys. Rev. B 21 (9) (1980) 3976–3998, https://doi.org/10.1103/PhysRevB.21.3976.
[49] A. Tekgül, Ö. Çaklr, M. Acet, M. Farle, N. Ünal, The structural, magnetic, and magnetocaloric properties of In-doped $Mn_{2-x}Cr_xSb$, J. Appl. Phys. 118 (2015), 153903, https://doi.org/10.1063/1.4934253.
[50] J. Fan, L. Pi, L. Zhang, W. Tong, L. Ling, B. Hong, Y. Shi, W. Zhang, D. Lu, Y. Zhang, Investigation of critical behavior in $Pr_{0.55}$ $Sr_{0.45}MnO_3$ by using the field dependence of magnetic entropy change, Appl. Phys. Lett. 98 (2011) 300–303, https://doi.org/10.1063/1.3554390.
[51] B. Widom, Equation of state in the neighborhood of the critical point, J. Chem. Phys. 43 (11) (1965) 3898–3905, https://doi.org/10.1063/1.1696618.
[52] J.M. Kosterlitz, The critical properties of two-dimensional xy model, J. Phys. C Solid State Phys. 7 (1974) 1046–1060, https://doi.org/10.1088/1751-8113/41/32/324021.